



Development and evaluation of a closed-loop z-axis control strategy for wire-and-arc-additive manufacturing using the process signal

Lennart Vincent Hölscher¹ · Thomas Hassel¹ · Hans Jürgen Maier¹

Received: 9 January 2023 / Accepted: 19 July 2023 / Published online: 28 July 2023
© The Author(s) 2023

Abstract

Wire-and-arc-additive manufacturing (WAAM) is an additive manufacturing technology with a high deposition rate. WAAM usually employs a layer wise build-up strategy. This makes it necessary to know the height of each deposited layer to determine the height the z-axis has to travel after each layer. Current bead geometry models (BGM) lead to variations, which can gradually accumulate over the layers. The present study focuses on the development of a closed-loop control system capable of keeping the contact tube working distance (CTWD) constant during short-circuit gas metal arc welding (GMAW) based WAAM. The algorithm calculates the CTWD based on the resistance during the short circuit. The closed-loop strategy is compared to an open-loop control strategy, which moves along a predefined height step after each layer. Using the proposed control strategy, WAAM becomes a fully automated process without the need for preliminary experiments to determine the height step. Only a short calibration slope is necessary for a complete closed-loop additive build-up. To study the influence of the control strategy on the workpiece the energy input, mechanical strength, microhardness, porosity, and microstructure were analyzed. It is shown that the CTWD of the open-loop deposited component increases slowly. Due to the novel control approach, this is prevented by the closed-loop control, while the mechanical strength and microhardness remain.

Keywords Height step · Wire-and-arc-additive manufacturing · Gas-metal-arc welding · Process control · Closed-loop control

1 Introduction

Wire-and-arc-additive-manufacturing (WAAM) is an additive manufacturing technology, well suited for medium- to large-scale parts with medium or low complexity [1]. A wide variety of materials can be used for WAAM while maintaining the properties of conventionally manufactured components [2]. With steel, WAAM can achieve deposition rates usually ranging from 4 to 9 kg/h [3]. To ensure high deposition rates, interlayer cooling can be employed [4]. Most WAAM workpieces are built with gas-metal-arc-welding

(GMAW) [5]. WAAM mostly employs layer-wise build-up strategies. This means that the workpieces are cut into different layers. Between the layers, the torch must be lifted by the layer height. The layer height has to be determined by empirical studies, before building the workpiece [6]. The determined layer height is always only valid for one combination of process parameters such as wire feed, gas flow, travel speed, voltage, and interlayer dwell time.

Nowadays, process parameters for WAAM are planned using bead geometry models (BGM). Since the workpiece shape changes over the process, the heat conduction through the workpiece changes too. Consequently, the interlayer temperature through the build-up deviates. This usually leads to changing layer shapes and deeper penetration within the process. The bead height can be influenced by the inclination of overhanging structures within the workpiece [7]. Furthermore, the bead height is sensitive to arc current and voltage as well as shape distortion of the base plate [8]. It is reported that BGMs operate with an error rate of 5–10% [6]. Since WAAM works by overlapping the layers, this error accumulates through the build direction. Two possible problems can

✉ Lennart Vincent Hölscher
hoelscher@iw.uni-hannover.de

Thomas Hassel
hassel@iw.uni-hannover.de

Hans Jürgen Maier
maier@iw.uni-hannover.de

¹ Institut für Werkstoffkunde (Materials Science), Leibniz Universität Hannover, An der Universität 2, 30823 Garbsen, Germany

be caused by this error. If the layer height is determined too big, the nozzle to top surface distance (NTSD) will become too large, resulting in insufficient shielding gas coverage. If the layer height is determined too small, the welding process will produce a lot of spatters. In the worst case, the torch and the workpiece will collide [8, 9].

To ensure that a workpiece collision or insufficient shielding gas coverage does not occur, a closed-loop control is beneficial. Moreover, closed-loop control of the contact tube working distance (CTWD) can eliminate the need for BGMs, saving time and resources otherwise spent on preliminary studies. Closed-loop control can be accomplished by using external sensors, as it is done with charge-coupled device (CCD) cameras in [8, 10]. However, since external sensors increase the required space, increase the moving mass of the torch system, increase the costs, and may increase the build time, using the process signal as a sensor is a cheaper, faster, and lighter solution. In addition, external sensors limit the build directions by pointing to a specific point that is not coaxial with the wire. A 90° turn would result in the sensing point no longer pointing at the workpiece. Previous work has shown a significant correlation between the short-circuit resistance and the CTWD [11]. Therefore, the short-circuit resistance is used for the first time to control the CTWD in GMAW-WAAM.

The influence of the control strategy on the mechanical strength is studied. The porosity in workpieces also affect the mechanical properties as well [12]. It can dramatically increase, when the CTWD is too high. Microhardness is another factor influenced by the CTWD. The work of Henckell et al. shows a relationship between CTWD and hardness [13]. It is shown that higher CTWDs lead to a higher hardness [13].

2 Process control in WAAM

Several attempts to control WAAM have been described in literature. In [14], the authors control the layer width by varying the travel speed of the Cartesian moveable workpiece. The layer width is measured with a CCD camera using computer image processing. The authors consider that the process is nonlinear with multiple variables, which interfere. Therefore, a PID algorithm is not applicable. Instead, they use a single-neuron controller. The single-neuron controller adjusts its output according to an S-shaped function. The function adapts its shape using a learning algorithm. The system responded to a step change in layer width within 5 s. Most target weld bead widths could be achieved with a maximum absolute error of less than 0.5 mm [14]. In order to keep the camera pointed at the right spot, the camera must be reoriented each time the direction of travel is changed. This makes the system

vulnerable to changes in the torch's direction of travel. A system, which works coaxial with the process wire, could solve this issue.

Xu et al. use a digital light processing system to measure the three-dimensional geometry of the workpiece in robotic WAAM. The acquired data is used to adjust the speed of the torch. The evaluated workpiece consists of a thin wall with two slopes. The movement speed is adjusted in such a way that the height difference of 10 mm is even after 18 layers [15]. The digital light processing scans the workpiece after the deposition of one layer. This means that an adaption of the travel speed can only be achieved in the upcoming layer. A sensor system which detects the workpiece geometry on-line during welding can be beneficial.

Ščetinec et al. chose to use the arc current to calculate the CTWD. The CTWD is corrected after each layer on a computer numerical control (CNC) based WAAM machine. If the expected workpiece height deviates from the actual height by more than 3.5 mm, the following layers are replanned. By correcting the CTWD after each layer and replanning the process, the accuracy of the workpiece can be improved from a total height deviation of 6.8 to 0.1% [9]. By using the process current, the torch position can be sensed coaxially. However, using the short-circuit resistance is a more accurate method of sensing the CTWD.

A control of the deposition height on a stepper-motor driven WAAM machine is achieved in [8]. Therefore, Xiong et al. use a CCD camera with a narrow band filter and image processing techniques to acquire the NTSD. The NTSD is used to control the wire feed rate via an adaptive controller. The controller adjusts its parameters based on system identifications. This leads to a smoother NTSD distribution. The system is able to control the NTSD within a range of ± 0.5 mm [8]. Even though the system works in the given case, using this method on a different workpiece geometry can lead to collisions between the camera and the workpiece.

Reisgen et al. also use a CCD camera for controlling the deposition process on a CNC-based WAAM machine. The camera detects the wire stickout and processes an elevation map of the workpiece. Two different control strategies are tested, one controls the CTWD and the other control strategy controls the wire feed rate. The total height error can be reduced from 25 to 7%, when using both control strategies [10]. The control of the wire feed shows advantages to achieve a smaller height error, but the CCD camera is an easily disturbed measuring device and dependent on the build direction.

Another attempt in controlling the skeleton robotic WAAM process with a CCD camera is shown by Radel et al. The authors use a blur filter and a canny filter to form the contour of the last weld bead. The camera can sense the NTSD in a window of 10 mm \times 15 mm [16]. This system can work well for skeletal workpieces, but will run into the

same problems as other camera-based systems when building multi-bead workpieces.

A fuzzy-logic control system is implemented into a robotic WAAM system in [6]. The authors use a triangulated light sensor to measure the height of the workpiece after each layer. The aim is to adjust the travel speed according to the bead height of the underlying bead in the previous layer. This control strategy is applied to a workpiece of 15 layers and 4 beads per layer. It achieves a total height error of 0.14 mm [6]. The triangulated light sensor requires a scan duration after each deposited layer, which may increase the build time.

Mu et al. also use a triangulated light sensor to detect the geometric features of the previous weld bead. Based on these measurements, the parameters for wire feed rate and travel speed of the robot are determined. The geometry of the following weld bead is predicted using a self-trained model. The height difference in each layer decreases from 2 mm in the uncontrolled case to 0.5 mm in the controlled case [17]. The triangulated light sensor works in this case after the deposition of a layer, which may increase the build duration.

Most other works use external sensors, which work non-coaxial to the process wire. This makes them dependent on the travel direction of the torch. Moreover, these sensors are susceptible to failure due to shading. Therefore, it is beneficial to use a sensor, which works coaxially to the deposition. Additionally, sensors which can only work when the welding is stopped may increase the build duration. During the deposition, only the electrical process signal can be detected coaxially. Based on previous work, shown in [11], the contact-tube-to-working-distance (CTWD) can be interpreted based on the process signal. In [11], slopes have been welded and characteristic features were extracted out of the process signal. It was observed, that the resistance during short circuit has the highest correlation with the CTWD.

In this work, the short-circuit resistance is used as an input for a control scheme. A closed-loop controlled workpiece is fabricated and compared to a workpiece fabricated with the traditional build-up strategy. The energy per unit length, mechanical strength, porosity, microhardness, and microstructure are compared.

3 Material and methods

3.1 Experimental setup

The electric power was delivered by an EWM Titan XQ 400 pulse (EWM AG, Mündersbach, Germany) welding power source. The wire feed speed was set to 5.5 m/min. The power source adapts its current and voltage delivery appropriate to the wire feed speed. To lower the heat input, the power source job coldArc was selected. The voltage and current cycle of this job are described as shown in Fig. 1. The wire had a diameter of 0.8 mm and met the specifications of EN ISO 14341-A (2011) G42 4M21 3Si1. As the welding torch, the Abicor Binzel ROBO WH W 500 (Alexander Binzel Schweisstechnik GmbH & Co. KG, Buseck, Germany) was used. The voltage was measured between the torch and the workpiece. It was brought into the measurement range of the I/O-controller (NI USB-6361 (NI, Austin, USA)) using a voltage divider with a resistance ratio of 1:5. The current was measured using a Chauvin Arnoux PAC22 (Chauvin Arnoux, Paris, France) current measurement clamp. The experimental setup is shown in Fig. 2. All welding related parameters are listed in Table 1.

The drive system featured four stepper motors. Two motors drove the x-axis, one drove the y-axis, and another one drove the z-axis. The motors were controlled by a CNC system.

Fig. 1 Voltage, current, and power trend of the coldArc process; arc burning phase in red, short-circuit phase in green

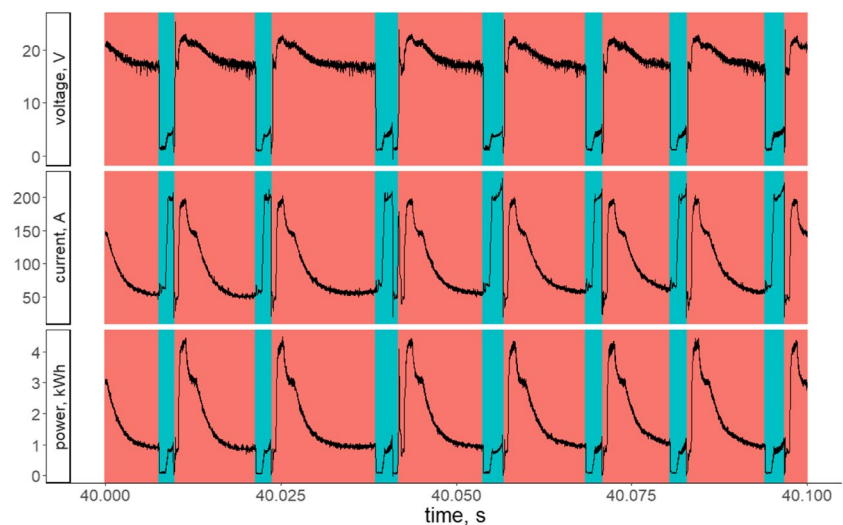
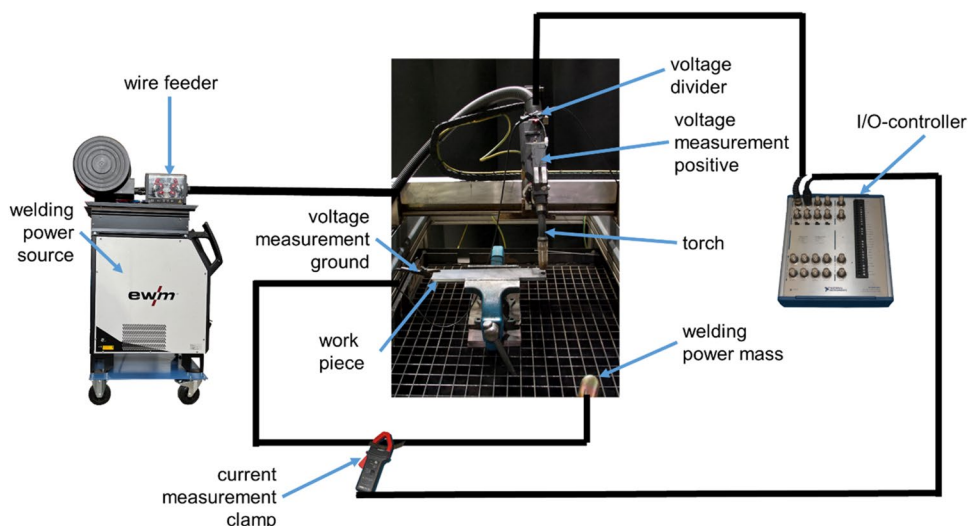


Fig. 2 Experimental setup with workpiece clamping



Two components were built on S355 steel substrate with the dimensions 300 mm × 80 mm × 10 mm. The substrates were clamped in a vise, as shown in Fig. 2. The samples were manufactured by moving the torch back and forth over a length of 280 mm. This resulted in a wall-shaped component. The target height was 90 mm. The layers are deposited bidirectional, as the arc starting and stopping points are switched after each layer. After the deposition of one layer, an inter-layer idle time of 60 s was kept. To mitigate start effects, the torch remains stationary at the starting point for 0.5 s after the process initiates. Similarly, when reaching the end point of each layer, the torch is held stationary for 0.5 s before turning off the arc.

The open-loop controlled component was manufactured by raising the z-axis along a predetermined distance after every layer. In the closed-loop control, the external controller drove the z-axis. In the open-loop control, the shape was sliced with the predefined height step into a given number of layers. In the closed-loop control, the controller was programmed to stop the welding process once the target height is achieved.

After the components were built, the resulting width and height were measured using a caliper gauge. To study the influence of the control loop on the quality of the manufactured workpieces, the components were cut using waterjet cutting and diamond wet cutting, as shown in Fig. 3. Microstructure test specimens were embedded, ground longitudinally, polished, and etched with nitric acid. The microstructure was captured using the light microscope Olympus BX53 (Olympus K.K., Tokyo, Japan). The grain sizes were then determined using digital image analysis. The microhardness test specimens were cut out using diamond wet cutting. The microhardness was tested according to DIN EN ISO 6507-1 along build-up direction with HV1 using a hardness tester type QATM Qness Q10 A+ (ATM Qness GmbH, Mammelzen, Germany). The

Table 1 Welding parameters

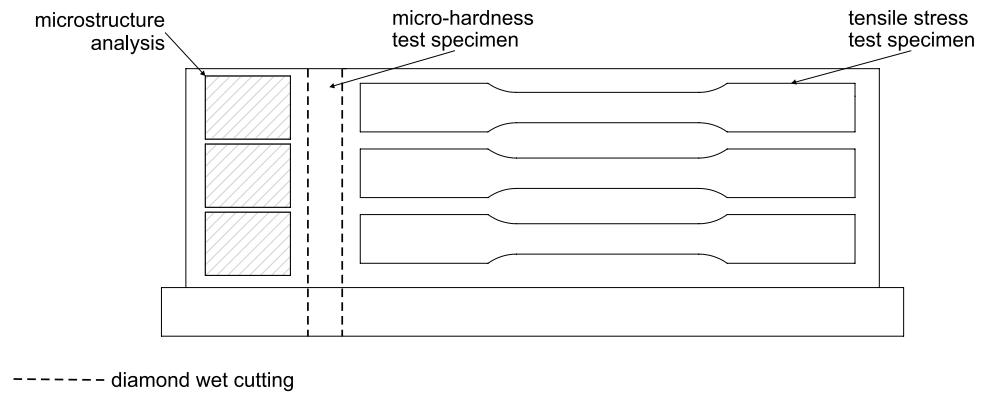
Parameter	Value
Power source	EWM Titan XQ 400 puls
Welding voltage	16.8 V
Welding torch	Abicor Binzel ROBO WH W 500
Wire material	EN ISO 14341-A (2011) G42 4M21 3Si1
Wire diameter	0.8 mm
Wire feed rate	5.5 m/min
Contact-Tube-Work-Distance	17.5 mm
Shielding gas	ISO 14175 M21 (Ar-CO ₂ 82-18)
Shielding gas flow	12 l/min
Substrate material	Mild steel (S355)
Welding speed	0.3 m/min

tensile test specimens were water jet cut and milled so that they had a thickness of 3 mm. The geometry of the tensile test specimens is based on DIN 50125 type E. The upper parts of the micro-hardness test specimens were X-ray scanned using a Zeiss Xradia 520 Versa (Carl Zeiss Microscopy GmbH, Jena, Germany). The specimens were cut at different heights to study if the height affected the tensile strength. The specimens were then tested using a Zwick Roell Z100 (ZwickRoell GmbH & Co. KG, Ulm, Germany) uniaxial tensile testing machine.

3.2 Open-loop control

The open-loop control strategy necessitates taking a constant height step after each layer to move forward. The height step was determined by welding five consecutive layers with a height step of 1.2 mm and a 60-s inter-layer idle time. The height of the 5 layers was 10 mm. This means that the average layer height of these layers is 2 mm. Hence, the height step is set to 2 mm. A

Fig. 3 Wall-shaped component with sample preparation



workpiece with a height of 90 mm was planned. This led to 40 additional layers, which were then manufactured on top of the existing 5 layers.

3.3 Closed-loop control

Initially, a value which is correlated with the CTWD had to be acquired. The work presented in [11] demonstrates that the CTWD in short-circuit gas-metal-arc welding (GMAW-S) is correlated with the resistance during short-circuiting. To apply this detection method to the energy-reduced coldArc process, a threshold voltage, which divides the signal in short-circuit and arc phase, needs to be identified. This was done by raising the CTWD from 5 to 30 mm during welding over a length of 60 mm. The voltage and current were recorded simultaneously at a measurement frequency of 50,000 Hz. The voltage value with the least occurrences between the arc voltage and the short-circuit voltage was chosen to be the threshold value. In the present case, a threshold voltage value of 11 V defined the short circuit. The density of the voltage occurrences together with the threshold voltage is illustrated in Fig. 4.

Since the short-circuit duration of a coldArc process is shorter than it is with GMAW-S, the minimum duration for the short-circuit detection had to be adapted. The minimum short-circuit duration was determined to be at least 0.75 ms.

The values were then fed into a proportional element, which calculated the distance to raise the torch based on the measured resistance required to keep the CTWD constant. To reduce variation, the resistance values were smoothed by applying a moving average filter with a sliding window length of 30 values. The resulting values were then fitted to a linear function, where R_{sc} is the short-circuit resistance (Eq. 1), using the method of least squares. A comparison of the calculated short circuit resistance with the measured short-circuit resistance (R_{sc}) against the CTWD is shown in Fig 5.

$$CTWD(R_{sc}) = 590.6 \frac{mm}{\Omega} * R_{sc} - 2.2 mm \quad (Eq. 1)$$

This strategy provides a CTWD determination with a standard deviation of ± 0.62 mm. Subsequently, the distance was converted into a number of steps that the stepper motor needed to travel in order to compensate for the deviation. To prevent the controller from raising the torch too high due to disturbances, the maximum number of steps per cycle was set to 800 steps.

The sample rate of the I/O-controller was set to 50,000 Hz. To average multiple short-circuit events, the voltage and current data were recorded for 850 ms while the z-axis correction steps were performed. Following that, the recorded data were analyzed and processed to determine

Fig. 4 Kernel density estimation of the welding voltage used for the definition of the threshold voltage

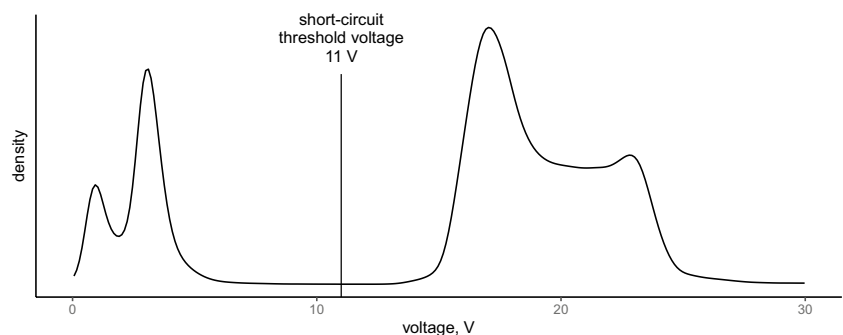
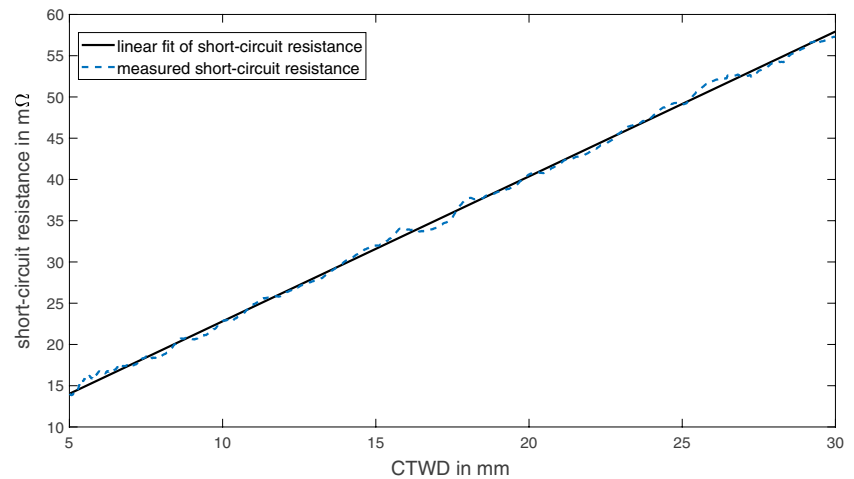


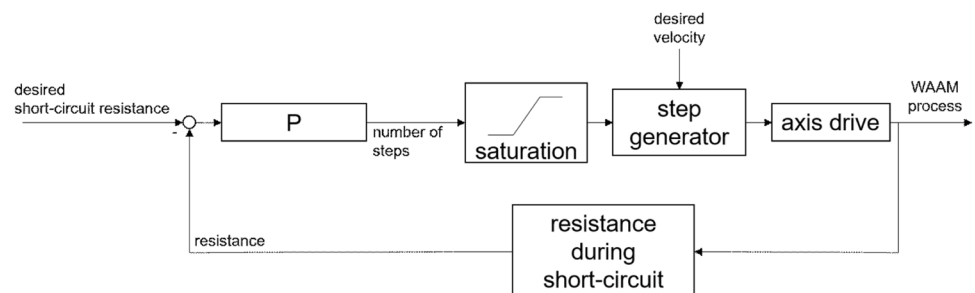
Fig. 5 Comparison between the expected short-circuit resistance and the measured short-circuit resistance



the average short-circuit resistance. The known short-circuit resistance for a CTWD of 17.5 mm is compared to the measured resistances. A proportional controller (labeled with “P” in Fig 6) uses the resulting difference and the coefficient $590.6 \frac{\text{mm}}{\Omega}$ of Eq. 1 as gain value to calculate the necessary number of steps to compensate. To prevent the axis from overshooting due to misdetection of the short-circuit resistance, a saturation element was programmed to allow a maximum axis movement of 3 mm per cycle. Once the number of steps was calculated, the square wave signal was generated at a frequency of 2667 Hz. This resulted in a travel speed of 10 mm/s. During the output of the square wave signal, the voltage and current data were recorded again. Since the processing took some time, the resulting refresh rate of the control loop was 0.8 Hz. The control loop is shown in Fig. 6.

The entire control loop, except for the axis drives, runs on a computer in a MATLAB environment. The square wave signal for the stepper motors is generated and passed via the analog output of the I/O-controller to the step amplifier (Fig. 7). Moreover, a directional signal is passed through a digital output towards the step amplifier. The step amplifier generates an electrical signal powerful enough to move the stepper motors. This signal flow is visualized in Fig. 7.

Fig. 6 Control loop for the z-axis



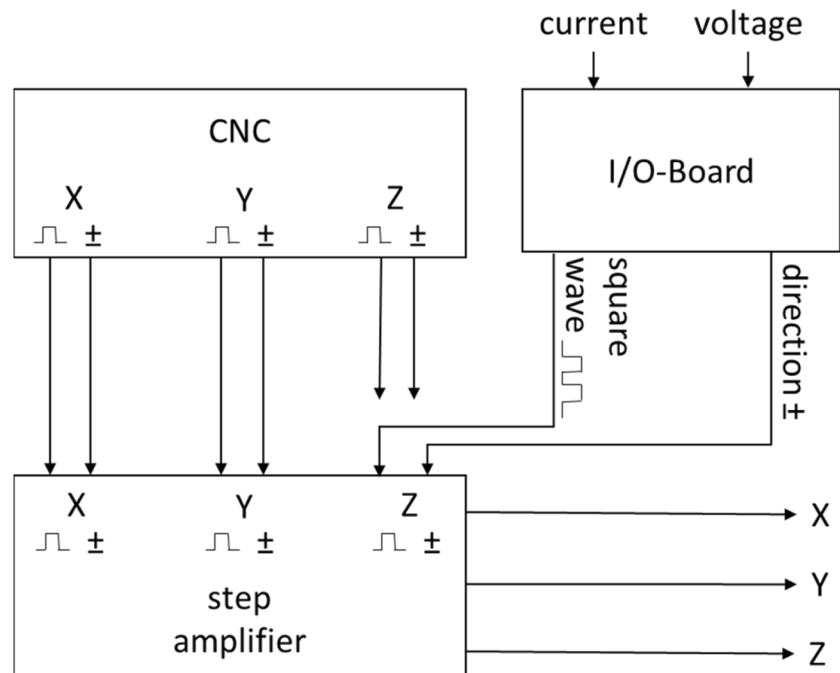
4 Results

4.1 Build process

Both components showed slight distortion due to the heat input. The width of both walls was 5.8 mm. The cross sections of the open-loop component showed a slightly narrower layer width in the upper layers, while the closed-loop controlled wall showed a more uniform cross section. The walls and their cross sections are shown in Fig. 8. Total build duration of the closed-loop control component was 99 min and 27 s, while the open-loop control took only 87 min 45 s. The pure welding time was 42 min 45 s for the open-loop component and 48 min 27 s for the closed-loop component. The open-loop control component featured 45 layers, while the closed-loop controlled component had 51 layers. Using the open-loop control strategy, a height in the middle of the component of 84.1 mm was achieved. As the component consists of 45 layers, the average layer height was 1.87 mm. The determined layer height was 2 mm (see section 3.2). The closed-loop control strategy resulted in a height at the middle of the component of 86.3 mm. These measurements are listed in Table 2.

The movement of the z-axis showed an overall increase. However, it did not show a linear or stepwise increase. The z-axis movement began with an alternating fall and rise

Fig. 7 Schematic drawing of electrical connections



followed by a continuously rising U-shaped function, as shown in Fig. 9.

The first layers show a clear decreasing axis position followed by a clear increasing axis position. It is noticeable that especially the first layers show an alternating trend behavior of the axis position. Later, during the manufacturing process, these increasing and decreasing trends resulted in a U-shape.

4.2 Energy input

The welding voltage and current data were also acquired and evaluated. To evaluate the energy input into the material, the energy per unit length was calculated for each layer. It is calculated as shown in Eq. 2, with U as voltage, I as current, and v as travel speed. The energy per unit length for each layer and control strategy is shown in Fig. 10.

$$E = \frac{U * I}{v} \quad (\text{Eq. 2})$$

Since the ignition and the end of the arc can cause misleading electrical measurements, the first and the last 5 s of the measurement were not considered. The energy per unit length during open-loop manufacturing increases in the first five layers, which were welded with a height step of 1.2 mm to determine the correct height step. The energy per unit length continued to decrease slowly in the remaining layers. The energy per unit length during the manufacturing of the closed-loop controlled component is higher in each layer. It varied between 272 and 282 J/mm.

Furthermore, the electrical signal was divided into arc and short circuit using the threshold voltage of 11 V and the minimum short-circuit duration of 0.75 ms. In Fig. 11, an increase in energy input is observed in the first five consecutive layers, followed by a steady decrease. An observation that can be made in Fig. 12 is that in the case of the open-loop controlled component, the energy per unit length during short-circuit decreases in the first five layers and increases in the remaining layers.

4.3 X-ray observations

The top of the microhardness test specimens was analyzed with an X-ray microscope. The pores in the top 45 mm are shown in Fig. 13. The observed porosity in the hardness specimen shows that there are pores with an average size of $300.61 \mu\text{m}^3$ in the open-loop controlled case. The specimen, which was built in a closed-loop manner, does not show any pores bigger than $0.48 \mu\text{m}^3$.

4.4 Mechanical strength

The yield strengths of the specimens were in a range between 390 and 417 MPa (see Fig. 14). A dependence of the yield strength on the position in the workpiece cannot be identified. The highest specimen of the open-loop controlled component showed the lowest tensile strength. This is due to the high amount of pores in the specimen. The high amount of pores lowers the cross section in which the load is applied and thereby leads to earlier failure. The tensile strengths of

Fig. 8 Manufactured walls with slightly different distortions visible: **a** open-loop control, **b** closed-loop control, **c** cross section of open-loop controlled component, **d** cross section of closed-loop controlled component

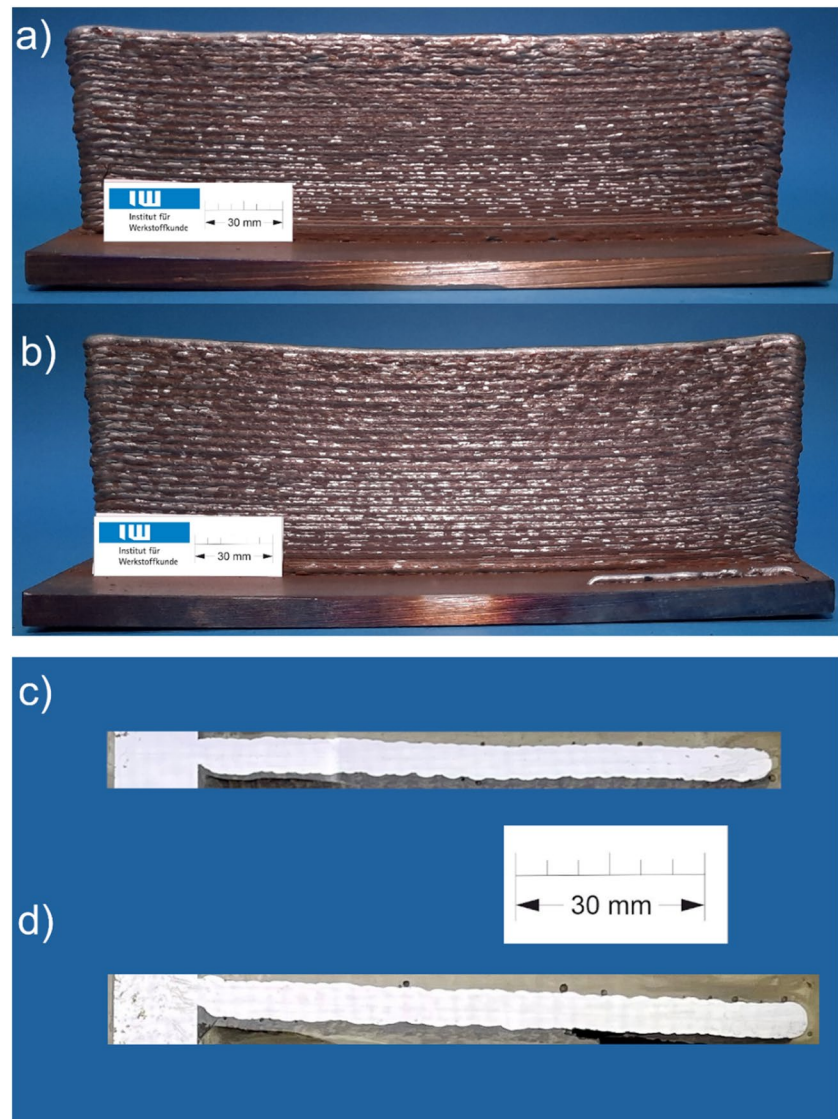


Table 2 Process times and geometries of the different components

	Open-loop	Closed-loop
Build duration	87 min 45 s	99 min 27 s
Welding duration	42 min 45 s	48 min 27 s
Height	84.1 mm	86.3 mm
Width	5.8 mm	5.8 mm
Layers	45	51

the pore-free samples are between 488 and 520 MPa, while elongation at break is between 17.5 and 19.7%.

4.5 Micro-hardness

In the first few layers and in the heat-affected zone of the substrate, a higher hardness than in the rest of the component

is observed. The hardness becomes constant in the middle of the component. At the end of the component, the hardness increases again due to the lack of annealing effects and a faster cooling rate. The average hardness of the closed-loop controlled component is 11 HV lower than the hardness of the open-loop controlled component. The microhardness evolution of the component along build-up direction is shown in Fig. 15.

4.6 Microstructure

The microstructure of all longitudinally ground samples consists mostly of ferrite with little perlite. Lack of fusion or pores are not visible in any of these images. Representative images of the microstructures are shown in Fig. 16.

The grain size was analyzed using a $100\ \mu\text{m} \times 5500\ \mu\text{m}$ microscope image of the specimen, as shown in Fig. 3. The microscope

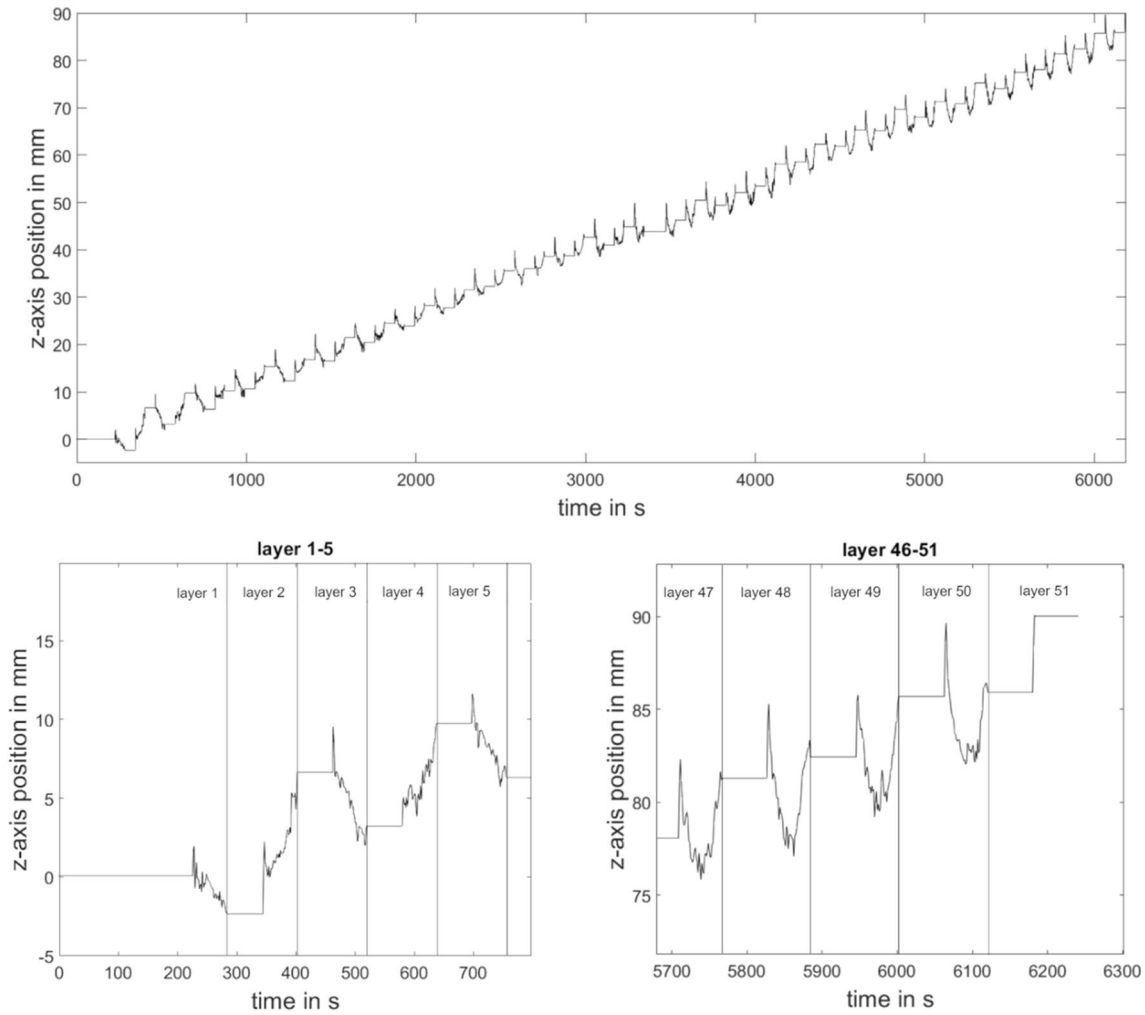
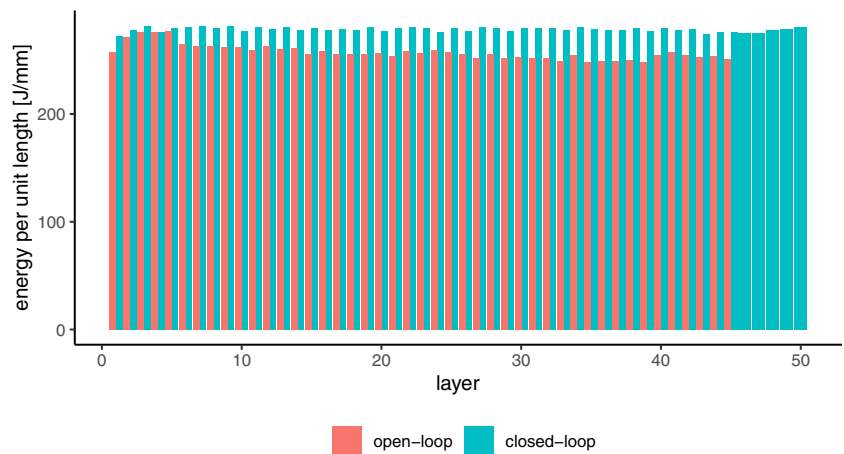


Fig. 9 z-Axis position during closed-loop manufacturing, layers 1–5 show an alternating z-axis position, while layers 46–51 show U-shaped z-axis motion

Fig. 10 Energy per unit length of both control loops; open-loop controlled component shows decreasing energy per unit length starting from layer 5



images included several manufactured layers; by using such a large area in z-direction, it can be ruled out that the grain size was measured within a welding typical coarse-grained zone. Nevertheless, measurement bias may occur due to different layer heights,

which may result in a different number of layers captured in the optical microscopy images. The grain size was analyzed using a morphological image filter. The grain size on the closed-loop manufactured workpiece is between 80.5 and 91.5 μm^2 . The

Fig. 11 Energy per unit length during arc; open-loop energy per unit length shows decreasing trend starting from layer 5

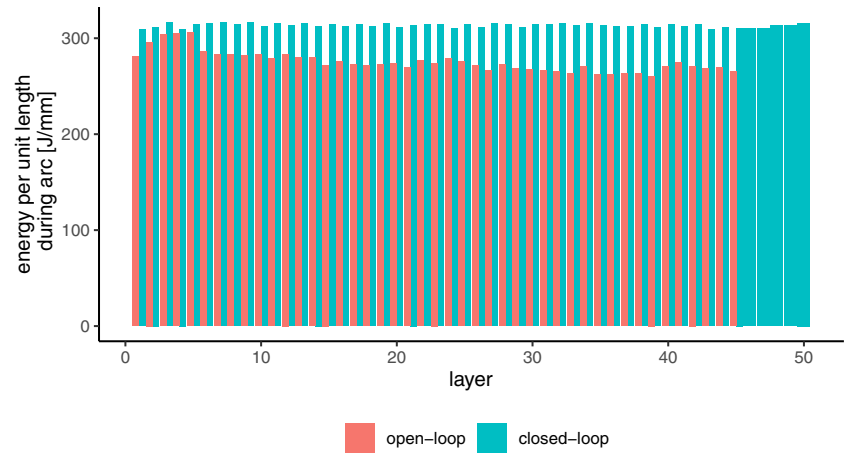


Fig. 12 Energy per unit length during short-circuit; open-loop energy per unit length shows increasing trend starting from layer 5

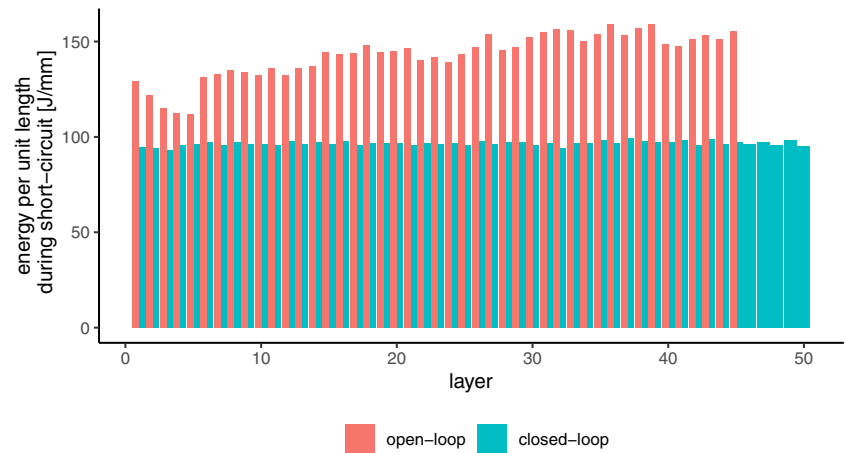
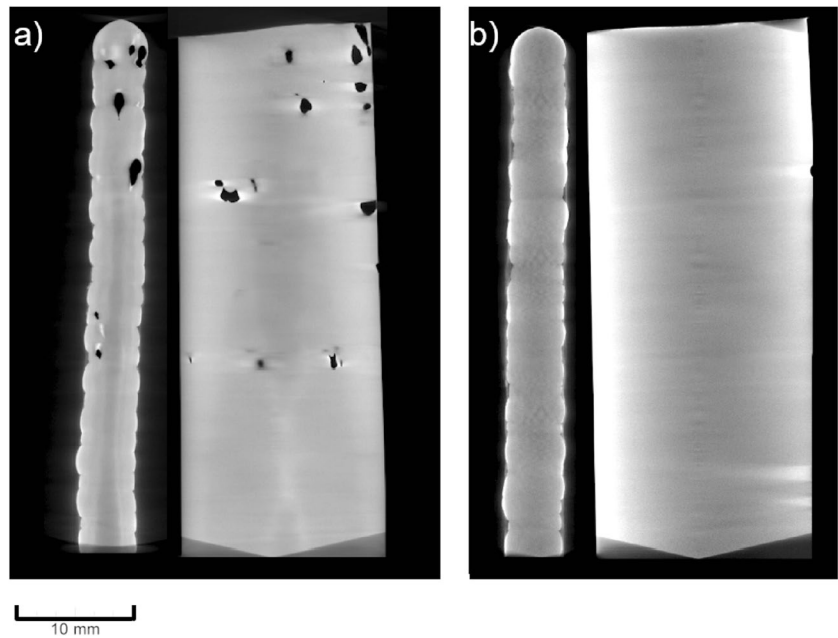


Fig. 13 **a** X-ray image of the open-loop workpiece shows pores; **b** X-ray image of the closed-loop workpiece shows no pores



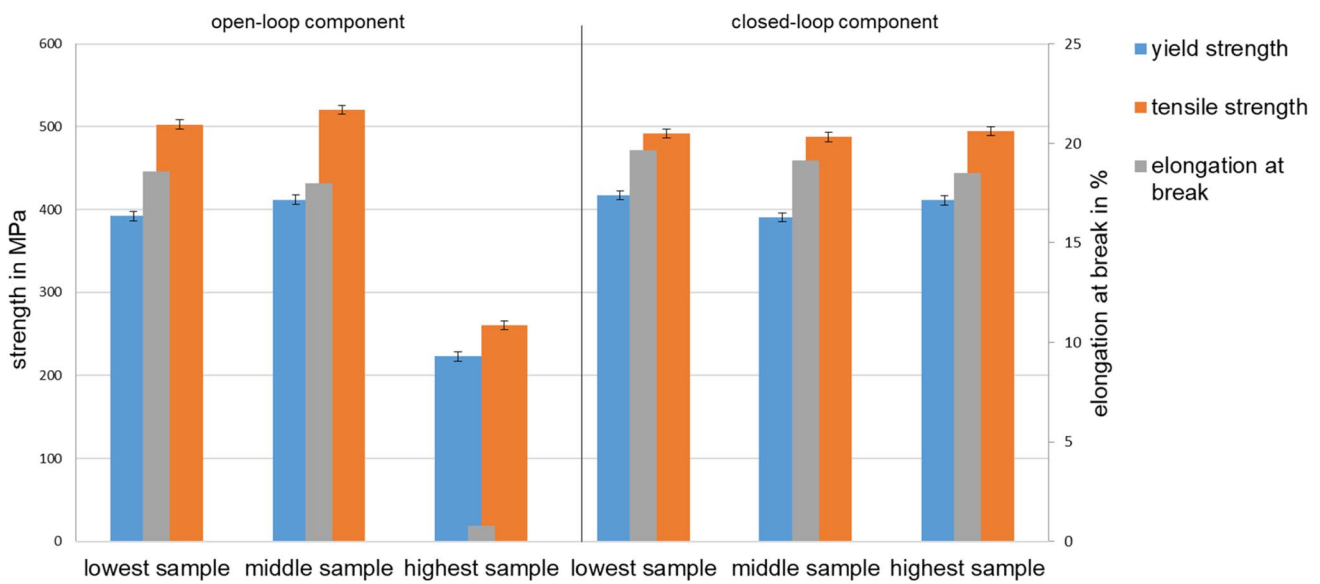
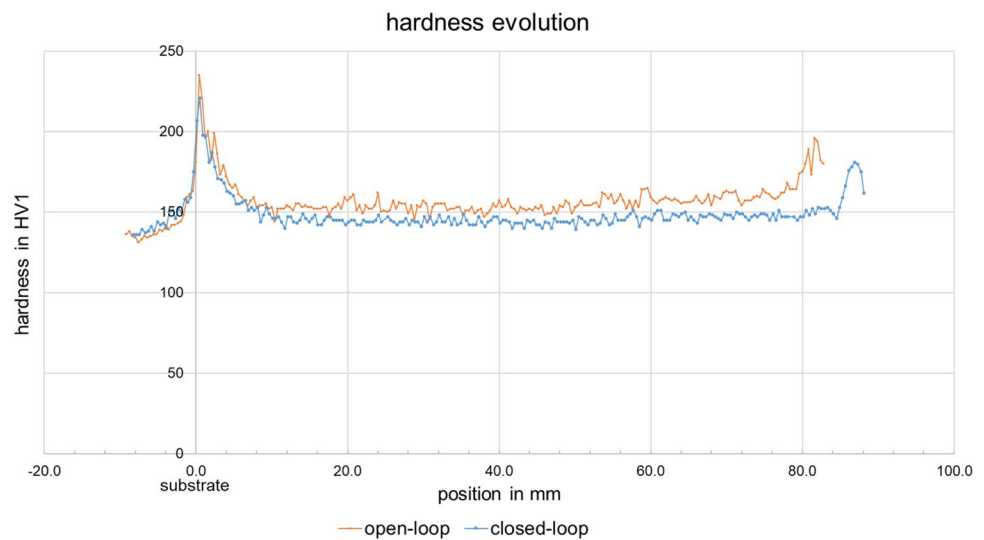


Fig. 14 Yield and tensile stresses of the different components with different heights; error bars indicate measurement accuracy of the testing device

Fig. 15 Hardness evolution for both components



open-loop controlled specimen showed a trend in the grain sizes. The grain size decreased towards the top of the component.

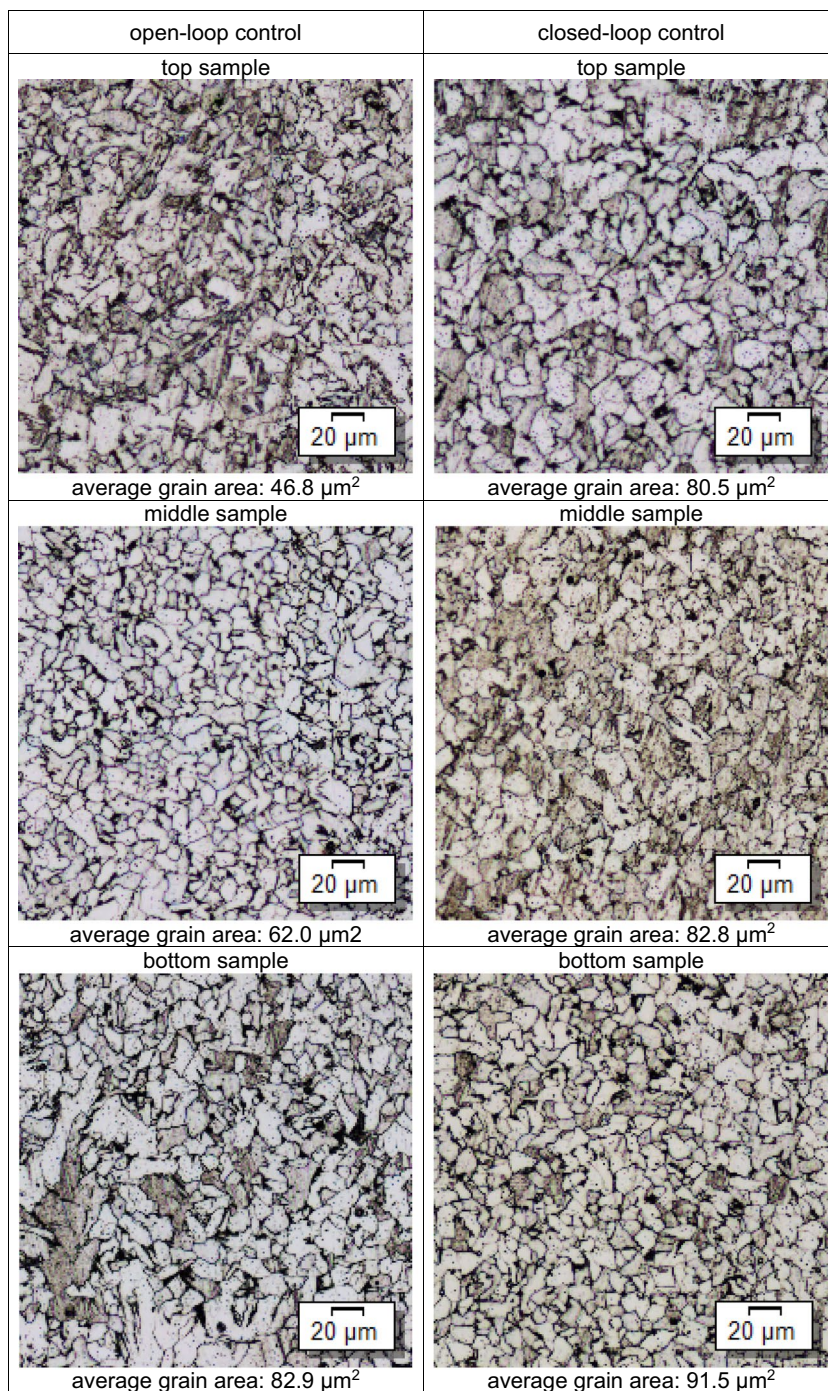
5 Discussion

The layer height of the open-loop component differed from the actual height step by 0.13 mm. This deviation was caused by the different heat fluxes in the first layers, which were used to determine the height step. The heat in the first layers can be easily conducted into the substrate plate. Thus, the first layers became higher. This effect biased the height step determination [18]. The difference between the actual layer

height and the traveled height step might result in higher CTWDs and less effective shielding gas conditions [8].

During each layer, the axis motion shows a characteristic trend of rising and falling. This cannot be caused by the changing distance to the voltage measurement clamp. Assuming that the current density is uniformly distributed over the entire cross section of the workpiece and that the resistivity of the workpiece and the wire are equal, the U-shape cannot be caused by the workpiece resistance because the area of the workpiece is 12,800 times larger than the conductive area of the wire. This means that a distance of 12,800 mm from the measuring clamp would cause a deviation of 1 mm in the misinterpreted CTWD. To further investigate this discrepancy, 50-mm-long tracks

Fig. 16 Microstructure cutouts



were welded to a new steel plate with the dimensions given in section 3.1. Both tracks were welded with a distance between the tracks of 255 mm. The measured CTWD of both beads is within ± 1 mm of the measurement accuracy. This was also the case when the workpiece was preheated to 75 °C. Therefore, it is clear that the workpiece resistance does not have a major influence on the CTWD detection. Even when the workpiece temperature was increased and the resistance increased, there was no deviation in the interpreted CTWD value.

The alternating behavior of rising and falling, however, suggests that the workpiece was not completely aligned straight to the torch. From Fig. 9, a difference of 2–3 mm can be seen between the start and end points. This could be explained by a tilt of 0.5°. The later change to U-shaped axis movements is due to thermal distortions the edges raise causing the start and stop points to be higher as the middle part. This can be observed in Fig. 8b. Another reason for the U-shape is the lower

wire resistance during the arc start. The conducting part of the wire is colder at the start of the process, since it was able to cool down during the inter-layer idle time. Moreover, the arc start sequence of the power source delivers a lower energy per unit length. A cold wire has a lower resistivity than a hotter one [19]. Lower wire resistances lead to CTWD misinterpreted too low, which let the z-axis move upwards.

In closed-loop controlled manufacturing, the controller was programmed to stop the manufacturing when the axis had moved by 90 mm and the layer was finished. Because the workpiece had geometric elevations at the start and stop points, and a height of 88.6 mm at these points, the previously discussed measurement variations resulted in axis movements that stopped manufacturing. Nevertheless, the closed-loop control strategy can improve the height accuracy.

Moreover, the energy input decreases during the manufacturing of the open-loop component. The energy input should be as low as possible since it leads to distortions, residual stresses, and coarse columnar grains [20, 21]. The decrease was caused by an increasing CTWD, which resulted in a longer wire extension. The wire acts as a resistance and limits the current flow, especially during the arc period. Lower energy per unit length at higher CTWDs is also observed in [22] and in [13]. In the first five layers the energy per unit length increases, during the first five layers the height step was determined with a height step of 1.2 mm. In the first five layers, the CTWD decreases with each layer. Moreover, the increase in energy per unit length during the short circuit is further proved for an increasing CTWD. To reignite the arc and form a droplet at the tip of the electrode, the EWM coldArc process needs to deliver an adequate amount of current to the wire tip. Since the wire acts as a resistance, a longer electrode extension requires a higher current to melt the wire tip.

Pores in the welded component may be caused by a lack of shielding gas [23]. It might be a result of the height step. While the torch gradually moved 2 mm in the height direction, the workpiece rose on average only 1.87 mm. This led to an average increase in CTWD of 0.13 mm per layer. Since every layer height can be different the exact CTWD increase per layer cannot be stated. The error accumulated over the 45 layers to 5.9 mm. Since the porosity starts at a height of 53.6 mm and the average layer height is 1.87 mm, the first layer, which is porous, is layer number 28. In layer number 28, the CTWD should be approximately 21.1 mm. Since it is unlikely that these CTWD already resulted in gas shielding issues, a partially clogged gas nozzle must also be part of the problem.

The hardness evolution of both components is typical for WAAM components and has also been shown by Henckell et al. [13]. This could be caused by the higher energy input into the workpiece caused by the lower CTWDs. This leads to lower cooling rates and bigger grain sizes (compare section 4.6). According to the Hall-Petch relationship, larger grains result in lower hardness.

The higher divergence in grain size for open-loop components is caused by the lower heat input due to the lower energy per unit length. This resulted in faster cooling rates, allowing smaller grains. The smaller grain size for samples with lower energy input and higher CTWDs is also observed in [13].

The measured tensile strength values are within the range as reported by [24, 25]. The samples demonstrate that the closed-loop control strategy is capable of producing workpieces with the same mechanical performance as with conventional methods.

Unlike the works of Radel, Reisgen, or Li have shown, WAAM process control can work without optical sensors [6, 10, 16], optical sensors are vulnerable to failure due to welding sparks and fumes. Moreover, they limit the build direction or torch movements, or extend the build duration.

Ščetinec et al. use the current during the arc existence as the parameter to determine the NTSD. This signal is highly distorted by a slope or a step in the workpiece. A slope or a step would lead in the first moment to an increased arc length and thereby a higher voltage. According to the constant voltage characteristic of the power sources, the current flow will increase, which leads to a wrong detection of the NTSDs. The authors encounter this problem by using an exponential moving average filter algorithms. The work by Ščetinec et al. shows a control loop which includes reslicing, which may be beneficial for workpieces with a more complex shape, for example, workpieces with overhanging parts [9].

The short-circuit resistance is well suited for the controlling of the CTWD. Based on the acquired data, it can be seen that the CTWD was constant throughout the whole manufacturing process. The control loop moreover is robust towards changes in workpiece temperature or workpiece height. Furthermore, the control loop is able to keep the energy per unit length constant.

6 Summary and outlook

The experiment shows that the build-up of a component by continuously monitoring and correcting the CTWD based on the measured short-circuit resistance is possible. While other sensors may limit the build directions, using the process signal as feedback to the controller does not limit the build directions. The workpiece height

accuracy can be improved with the proposed strategy. Moreover, a closed-loop CTWD control strategy can prevent collisions between the torch and the workpiece and will allow to identify geometric disturbances in case of overlap. The mechanical properties of the workpieces are not significantly affected by the control loop.

Another advantage of the CTWD monitoring is the allowance of repair welding even on convex surfaces. This was especially visible due to a lack of straightness in the base plate. The control loop was able to compensate for these height differences. Moreover, the control loop managed to keep the CTWD constant even through distortions in the workpiece.

The closed-loop control strategy lead towards a slightly higher energy input. This was caused by the overall lower CTWDs. However, the energy input across all layers can be kept constant with a closed-loop build strategy. The constant energy input results in a homogenous grain size. The increasing CTWDs in the open-loop component lead to a trend in smaller grain sizes toward the top of the component. Using the presented control strategy, new build strategies become possible, such as building workpieces in a continuous motion rather than layer-by-layer. For a tube-shaped component, this would result in a spiral motion. Today's slicing methods can be replaced by new adaptive slicing methods, which react to the actual workpiece shape.

Acknowledgements EWM AG is thanked for providing a state-of-the-art welding power source for these investigations.

Author contributions LVH, TH, and HJM conceptualized the work. TH and HJM supervised the study. LVH developed software, designed the experimental setup, ran the investigation, and wrote the original draft. TH and HJM acquired funding and revised the paper.

Funding Open Access funding enabled and organized by Projekt DEAL. Funded by the Ministry for Science and Culture of Lower Saxony (MWK) – School for Additive Manufacturing SAM.

Data, material, and/or code availability Measurement data, materials, and code can be obtained from the authors upon request.

Declarations

Conflict of interest The authors declare no competing interests.

Open Access This article is licensed under a Creative Commons Attribution 4.0 International License, which permits use, sharing, adaptation, distribution and reproduction in any medium or format, as long as you give appropriate credit to the original author(s) and the source, provide a link to the Creative Commons licence, and indicate if changes were made. The images or other third party material in this article are included in the article's Creative Commons licence, unless indicated otherwise in a credit line to the material. If material is not included in the article's Creative Commons licence and your intended use is not permitted by statutory regulation or exceeds the permitted use, you will need to obtain permission directly from the copyright holder. To view a copy of this licence, visit <http://creativecommons.org/licenses/by/4.0/>.

References

- Williams SW, Martina F, Addison AC et al (2016) Wire + arc additive manufacturing. *Mater Sci Technol* 32:641–647. <https://doi.org/10.1179/1743284715Y.0000000073>
- Treutler K, Wesling V (2021) The current state of research of wire arc additive manufacturing (WAAM): a review. *Appl Sci* 11:8619. <https://doi.org/10.3390/app11188619>
- Evans SI, Wang J, Qin J et al (2022) A review of WAAM for steel construction – manufacturing, material and geometric properties, design, and future directions. *Structures* 44:1506–1522. <https://doi.org/10.1016/j.istruc.2022.08.084>
- Tonelli L, Sola R, Laghi V et al (2021) Influence of interlayer forced air cooling on microstructure and mechanical properties of wire arc additively manufactured 304L austenitic stainless steel. *Steel Res Int* 92:2100175. <https://doi.org/10.1002/srin.202100175>
- Hauser T, Reisch RT, Breese PP et al (2021) Porosity in wire arc additive manufacturing of aluminium alloys. *Addit Manuf* 41:101993. <https://doi.org/10.1016/j.addma.2021.101993>
- Li Y, Li X, Zhang G et al (2021) Interlayer closed-loop control of forming geometries for wire and arc additive manufacturing based on fuzzy-logic inference. *J Manuf Process* 63:35–47. <https://doi.org/10.1016/j.jmapro.2020.04.009>
- Lam TF, Xiong Y, Dharmawan AG et al (2020) Adaptive process control implementation of wire arc additive manufacturing for thin-walled components with overhang features. *Int J Adv Manuf Technol* 108:1061–1071. <https://doi.org/10.1007/s00170-019-04737-4>
- Xiong J, Zhang G (2014) Adaptive control of deposited height in GMAW-based layer additive manufacturing. *J Mater Process Technol* 214:962–968. <https://doi.org/10.1016/j.jmatprotec.2013.11.014>
- Ščetinec A, Klobčar D, Bračun D (2021) In-process path replanning and online layer height control through deposition arc current for gas metal arc based additive manufacturing. *J Manuf Process* 64:1169–1179. <https://doi.org/10.1016/j.jmapro.2021.02.038>
- Reisgen U, Mann S, Oster L et al (2019) Study on workpiece and welding torch height control for polydirectional WAAM by means of image processing. In: *IEEE 15th International Conference on Automation Science and Engineering (CASE)*. IEEE
- Hölscher LV, Hassel T, Maier HJ (2022) Detection of the contact tube to working distance in wire and arc additive manufacturing. *Int J Adv Manuf Technol* 226:1042–1053. <https://doi.org/10.1007/s00170-022-08805-0>
- Cong B, Ding J, Williams S (2015) Effect of arc mode in cold metal transfer process on porosity of additively manufactured Al-6.3%Cu alloy. *Int J Adv Manuf Technol* 76:1593–1606. <https://doi.org/10.1007/s00170-014-6346-x>
- Henckell P, Gierth M, Ali Y et al (2020) Reduction of energy input in wire arc additive manufacturing (WAAM) with gas metal arc welding (GMAW). *Materials* 13:2491. <https://doi.org/10.3390/ma13112491>
- Xiong J, Yin Z, Zhang W (2016) Closed-loop control of variable layer width for thin-walled parts in wire and arc additive manufacturing. *J Mater Process Technol* 233:100–106. <https://doi.org/10.1016/j.jmatprotec.2016.02.021>
- Xu B, Tan X, Gu X et al (2019) Shape-driven control of layer height in robotic wire and arc additive manufacturing. *RPJ* 25:1637–1646. <https://doi.org/10.1108/RPJ-11-2018-0295>
- Radel S, Diourte A, Soulié F et al (2019) Skeleton arc additive manufacturing with closed loop control. *Addit Manuf* 26:106–116. <https://doi.org/10.1016/j.addma.2019.01.003>
- Mu H, Polden J, Li Y et al (2022) Layer-by-layer model-based adaptive control for wire arc additive manufacturing of thin-wall

- structures. *J Intell Manuf* 33:1165–1180. <https://doi.org/10.1007/s10845-022-01920-5>
18. Wu B, Pan Z, van Duin S et al (2019) Thermal behavior in wire arc additive manufacturing: characteristics, effects and control. *Transactions on Intelligent Welding Manu* 32:3–18. https://doi.org/10.1007/978-981-13-3651-5_1
 19. Zhang G, Goett G, Kozakov R et al (2019) Study of the wire resistance in gas metal arc welding. *J Phys D Appl Phys* 52:85201. <https://doi.org/10.1088/1361-6463/aaf5bb>
 20. Li Z, Liu C, Xu T et al (2019) Reducing arc heat input and obtaining equiaxed grains by hot-wire method during arc additive manufacturing titanium alloy. *Mater Sci Eng A* 742:287–294. <https://doi.org/10.1016/j.msea.2018.11.022>
 21. Rodrigues TA, Duarte V, Miranda RM et al (2019) Current status and perspectives on wire and arc additive manufacturing (WAAM). *Materials (Basel)* 12:1121. <https://doi.org/10.3390/ma12071121>
 22. Haelsig A, Kusch M, Mayr P (2015) Calorimetric analyses of the comprehensive heat flow for gas metal arc welding. *Weld World* 59:191–199. <https://doi.org/10.1007/s40194-014-0193-0>
 23. Dilthey U, Brandenburg A (2002) *Schweißtechnische Fertigungsverfahren 2: Gestaltung und Festigkeit von Schweißkonstruktionen*, 2. überarbeitete Auflage. VDI-Buch. Springer, Berlin, Heidelberg
 24. Ghaffari M, Vahedi Nemani A, Rafieezad M et al (2019) Effect of solidification defects and HAZ softening on the anisotropic mechanical properties of a wire arc additive-manufactured low-carbon low-alloy steel part. *JOM* 71:4215–4224. <https://doi.org/10.1007/s11837-019-03773-5>
 25. Reimann J, Hammer S, Henckell P et al (2021) Directed energy deposition-arc (DED-Arc) and numerical welding simulation as a hybrid data source for future machine learning applications. *Appl Sci* 11:7075. <https://doi.org/10.3390/app11157075>

Publisher's note Springer Nature remains neutral with regard to jurisdictional claims in published maps and institutional affiliations.